Breaking the Entangling Gate Speed Limit for Trapped-Ion Qubits Using a Phase-Stable Standing Wave

S. Saner,[*,‡] O. Băzăvan,[†,‡] M. Minder, P. Drmota, D. J. Webb, G. Araneda, R. Srinivas, D. M. Lucas, and C. J. Ballance

Department of Physics, University of Oxford, Clarendon Laboratory, Parks Road, Oxford OX1 3PU, United Kingdom

(Received 31 May 2023; accepted 16 October 2023; published 1 December 2023)

All laser-driven entangling operations for trapped-ion qubits have hitherto been performed without control of the optical phase of the light field, which precludes independent tuning of the carrier and motional coupling. By placing $^{88}Sr^{+}$ ions in a $\lambda = 674$ nm standing wave, whose relative position is controlled to $\approx\lambda/100$, we suppress the carrier coupling by a factor of 18, while coherently enhancing the spin-motion coupling. We experimentally demonstrate that the off-resonant carrier coupling imposes a speed limit for conventional traveling-wave Mølmer-Sørensen gates; we use the standing wave to surpass this limit and achieve a gate duration of 15 μs, restricted by the available laser power.

DOI: 10.1103/PhysRevLett.131.220601

Controlled light-matter interactions are essential for quantum computing [1–3], quantum simulation [4,5], and metrology [6,7]. For trapped ions, these applications typically require carrier interactions that only couple internal qubit states, as well as sideband interactions that couple these internal states to their collective motion [3]. For example, the sideband interactions, driven by the spatial gradient of the carrier coupling, are used to mediate spin-spin interactions such as entangling gates [8]. Conventionally, coherent control of laser-ion interactions is achieved using traveling waves (TWs) [3]. As the ions experience an averaged electric field and gradient over the interaction duration, the ratio between carrier coupling and sideband coupling is fixed. In contrast, the coupling strengths for ions in a standing wave (SW) vary with the spatial structure of the light field along its propagation direction. Consequently, the phase of the SW at the ions sets the ratio between the carrier and sideband coupling. Coherent SW interactions on a single ion have been studied previously using cavities [9,10], integrated optics [11], and free-space approaches [12]. However, coherent operations on multiple ions with a SW have so far been unexplored.

The tunability of the carrier-sideband coupling ratio is especially important for strong interactions where off-resonant terms start participating significantly and cannot be eliminated adiabatically. For example, in the conventional Mølmer-Sørensen (MS) mechanism [13], the TW that generates the spin-motion coupling also gives rise to an off-resonant carrier coupling, which causes an error in the entangling operation. This error becomes significant as the carrier interaction strength approaches the motional frequency, placing a limit on the speed of the entangling operation. Using a SW instead enables high-fidelity entangling operations that can surpass this speed limit by selectively enhancing the spin-motion coupling while coherently suppressing the detrimental carrier term [14]. Fast entanglement generation is important for increasing the clock speed in trapped-ion quantum processors [3,15,16] and could enable experimental studies of vacuum entanglement and the propagation of quantum correlations in ion chains [17,18]. Furthermore, being able to tune the carrier-sideband ratio as a function of the position unlocks opportunities in metrology, such as sensing beyond the diffraction limit [19,20] or suppressing dipole light shifts when probing quadrupole clock transitions [21]. Standing waves may also be used for deterministic generation of entanglement in a quantum network [22].

In this Letter, we use a free-space, phase-stabilized SW to implement single- and two-qubit gates. The SW is formed by two superimposed counterpropagating 674-nm beams that couple to the quadrupole qubit transition, $5S_{1/2} \leftrightarrow 4D_{5/2}$, in $^{88}Sr^{+}$. The single-qubit gate is created using a monochromatic SW on resonance with the qubit transition while placing the node(s) of the SW at the position of the ion(s). The two-qubit entangling gate is implemented via an MS-type scheme where we use a bichromatic SW instead of the conventional bichromatic TW. We show that the presence of the carrier term, in the context of the TW-MS gate, leads to a reduction in the spin-dependent force (SDF) magnitude, which scales with the Rabi frequency of this detrimental term, posing an inherent speed limit for this mechanism. Using the SW-MS instead,

with the antinodes placed at the ions, we strongly suppress the undesired carrier term and show that we can surpass this speed limit.

To understand the interaction between a string of ions and a monochromatic SW driving a quadrupole transition, we consider two counterpropagating beams with Rabi frequency Ω, detuning δ from the qubit resonance, and a tunable phase difference $\Delta\phi = \phi_1 - \phi_2$ that is common to all (equally spaced) ions in the chain [23–25]. The resulting interaction is

$$\hat{H}_{\mathrm{SW}} = e^{-i\delta t}\hbar\eta\Omega\hat{S}_{+}e^{i\tilde{\phi}}(\hat{a}e^{-i\omega_z t} + \hat{a}^{\dagger}e^{i\omega_z t})\cos(\Delta\phi/2) + e^{-i\delta t}\hbar\Omega\hat{S}_{+}e^{i\tilde{\phi}}\sin(\Delta\phi/2) + \mathrm{H.c.}, \quad (1)$$

where η denotes the Lamb-Dicke factor, the average phase $\tilde{\phi} = (\phi_1 + \phi_2 + \pi)/2$, the spin-operator [26] for n ions is $\hat{S}_{+} = \sum_{i=1}^{n}\hat{\sigma}_{+}^{(i)}$, and $\hat{a}^{\dagger}$ ($\hat{a}$) denotes the creation (annihilation) operator of the motional mode [27]. This expression is in the interaction picture with respect to the qubit frequency ω_0, and the motional mode frequency ω_z, after the rotating wave approximation with respect to ω_0. By setting $\delta = 0$ or $\delta = \pm\omega_z$, we can bring the carrier or sidebands into resonance, respectively. With $\Delta\phi$ the SW has an additional degree of freedom compared to the TW: by setting $\Delta\phi = 0$ we can drive the first sidebands while suppressing all even terms in the Lamb-Dicke expansion [27], including the carrier term. Conversely, if we set $\Delta\phi = \pi$ we drive the carrier coupling and suppress all odd terms in the Lamb-Dicke expansion, including the first sidebands.

The MS interaction requires two tones symmetrically detuned about the qubit resonance by $\delta \approx \pm\omega_z$. To construct the Hamiltonian for a SW-MS interaction, we combine two monochromatic SWs as described by Eq. (1), resulting in the bichromatic SW interaction

$$\hat{H}_{\mathrm{SW-MS}} = 2\hbar\eta\Omega\hat{S}_{\tilde{\phi}}\cos(\delta t)(\hat{a}e^{-i\omega_z t} + \hat{a}^{\dagger}e^{i\omega_z t})\cos(\Delta\phi/2) + 2\hbar\Omega\hat{S}_{\tilde{\phi}}\cos(\delta t)\sin(\Delta\phi/2), \quad (2)$$

where the spin-operator for n ions is $\hat{S}_{\tilde{\phi}} = \sum_{i=1}^{n}\hat{\sigma}_{\tilde{\phi}}^{(i)}$ with $\hat{\sigma}_{\tilde{\phi}}^{(i)} = \hat{\sigma}_x^{(i)}\cos\tilde{\phi} + \hat{\sigma}_y^{(i)}\sin\tilde{\phi}$ and the phase $\tilde{\phi} = (\tilde{\phi}_{\mathrm{BD}} + \tilde{\phi}_{\mathrm{RD}})/2$ is the mean optical phase between the blue- (BD) and the red- (RD) detuned SWs. Further, we assume that the BD and RD SWs are in phase at the position of the ion(s), i.e. $\Delta\phi_{\mathrm{BD}} = \Delta\phi_{\mathrm{RD}} = \Delta\phi$. The first term corresponds to a SDF and the second term drives the carrier transition off-resonantly. Notably, these terms commute. Similar to the monochromatic SW, we can drive the motional coupling while suppressing the spurious carrier coupling by setting $\Delta\phi = 0$.

The advantage of using a SW-MS interaction becomes evident when considering the conventional MS scheme, which consists of a BD and RD TW at $\delta \approx \pm\omega_z$:

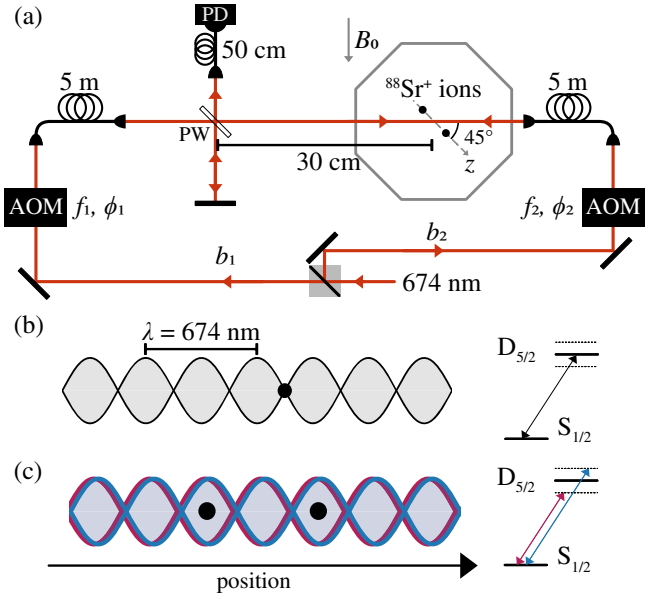

FIG. 1. (a) Schematic of the experimental apparatus. The incoming 674-nm beam is split into two beams (b_1, b_2). The acousto-optic modulators (AOMs) are used to control the frequencies (f_1, f_2) and phases (ϕ_1, ϕ_2) of the two counterpropagating beams, which have polarization parallel to B_0 and equal intensities at the ions. We close the resulting interferometer with a pick-off window (PW) ≈ 30 cm away from the ion(s). For fast feedback (see text) we stabilize the interference fringe intensity on a photodiode (PD) by adjusting ϕ_1. (b) Monochromatic resonant SW for single-qubit rotations. (c) Bichromatic off-resonant SW for two-qubit gates.

$$\hat{H}_{\mathrm{TW-MS}} = \hbar\eta\Omega\hat{S}_{\phi}\cos(\delta t)(\hat{a}e^{-i\omega_z t} + \hat{a}^{\dagger}e^{i\omega_z t}) + \hbar\Omega\hat{S}_{\phi-\pi/2}\cos(\delta t), \quad (3)$$

where ϕ is the mean optical phase between the BD and RD TWs. Crucially, in this case, the carrier and the SDF terms no longer commute. Hence, when using this SDF to implement a two-qubit entangling gate, the off-resonant carrier coupling introduces an error, which increases with Ω. This error can be partially mitigated by adiabatic ramping of the interaction (i.e., amplitude pulse shaping), which ensures a smooth transition into the interaction picture with respect to the carrier coupling if $\Omega \lesssim \delta$. Nevertheless, the noncommuting carrier term effectively limits the speed of entangling operations because it saturates the achievable SDF magnitude. By moving into the interaction picture with respect to the carrier term [28–30], Eq. (3) becomes

$$\hat{H}^{I}_{\mathrm{TW-MS}} = \hbar\Omega_{\mathrm{SDF}}\cos(\delta t)\hat{S}_{\phi}(\hat{a}e^{-i\omega_z t} + \hat{a}^{\dagger}e^{i\omega_z t}),$$
$$\Omega_{\mathrm{SDF}}(\Omega,\delta) = \eta\Omega[J_0(2\Omega/\delta) + J_2(2\Omega/\delta)], \quad (4)$$

where J_0 and J_2 are Bessel functions of the first kind. The effective coupling strength Ω_{SDF} has a global maximum

which limits the gate speed even if Ω is further increased (e.g. by increasing the laser power).

We experimentally compare single- and two-qubit operations implemented via SWs or TWs using the setup shown in Fig. 1(a). We trap one or two $^{88}Sr^{+}$ ions in a 3D radio-frequency Paul trap [31,32] with a quantization axis defined by a magnetic field B_0. Our qubit is encoded in $|\downarrow\rangle \equiv |5S_{1/2}, m_j = -\frac{1}{2}\rangle$ and $|\uparrow\rangle \equiv |4D_{5/2}, m_j = -\frac{3}{2}\rangle$; we address the quadrupole qubit transition using a 674-nm laser. The laser output is split into two beams, b_1 and b_2. Both beams have a $\approx$21 μm waist radius at the ion position. For experiments with a TW we use b_1 alone. To generate a free-space SW, light from both beams is aligned in a counterpropagating geometry onto the ions. The beams make an angle of $\approx$45° to the trap z axis resulting in an ion separation projected on the SW axis of $\approx 3.8\,\mu\text{m} \cdot \cos(45°) = 4\lambda$.

To perform coherent operations with the SW, we need to control the phase $\Delta\phi$ at the position of the ion(s), which is achieved by adjusting phase ϕ_1. We increase the passive stability of $\Delta\phi$ with an enclosure around the free-space optical paths. Additionally, we actively stabilize $\Delta\phi$ on two timescales: fast feedback derived from optical interference sampled near the position of the ions, and slow feedback derived from Ramsey experiments on the ion(s) [27]. Using a single ion as a sensor, we observe residual phase fluctuations with an rms deviation of $\approx$0.12 rad (position fluctuations of $\approx\lambda/100$) over one hour. This is near the shot noise limit, i.e. 0.10 rad for 100 shots of feedback.

We probe the position of the SW relative to a single ion by applying a monochromatic SW pulse on resonance with the qubit transition [Figs. 1(b) and 2(a)]. The pulse duration corresponds to a π pulse at maximum carrier coupling. As we are driving an electric quadrupole transition, this maximum occurs at the nodes of the SW, where the gradient of the electric field has the largest amplitude [9]. Conversely, the sideband coupling is maximized at the antinodes of the SW as it is proportional to the spatial derivative of the carrier coupling along the motional direction. Hence, we can maximize the carrier and minimize the sideband coupling, or vice versa, by selecting $\Delta\phi = \pi$ or $\Delta\phi = 0$ [Fig. 2(b)]. The transfer probability shown in Fig. 2(a) has a quartic dependence on $\Delta\phi$ near $\Delta\phi = \pi$ and a quadratic dependence near $\Delta\phi = 0$ [27]. When probing the suppressed motional sideband [Fig. 2(b) left], we observe only features that are due to the off-resonant (by $\approx$1.2 MHz) carrier coupling. By changing $\Delta\phi$, we can realize any ratio between carrier and sideband coupling.

We measure Rabi frequencies by scanning the SW pulse duration at the carrier resonance, for both $\Delta\phi = \pi$ and $\Delta\phi = 0$. We observe this ratio to be 18, corresponding to a suppression of 25 dB between maximal and minimal carrier coupling. This suppression is consistent with the measured interferometric stability and the residual power imbalance

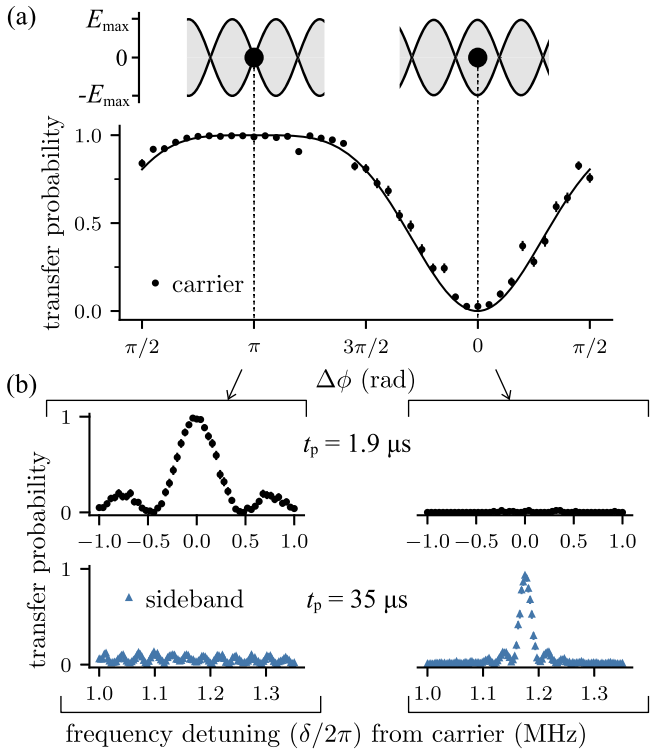

FIG. 2. Monochromatic SW interacting with a single ion. (a) Qubit state transfer probability as a function of the SW phase at the ion position, while the SW is resonant with the carrier. We indicate the ion positions in the SW that maximize ($\Delta\phi = \pi$) or minimize ($\Delta\phi = 0$) the carrier coupling for a quadrupole transition. The SW pulse duration t_p is set such that complete population transfer is achieved at maximal carrier coupling. (b) Detuning scans over carrier (circles) and motional sideband (triangles) resonance while placing the ion at a field node (left column) or field antinode (right column). For each resonance, t_p is chosen such that full population transfer is reached in the case of maximal coupling to the SW.

between b_1 and b_2. Furthermore, we perform randomized benchmarking [33] to evaluate the quality of single-qubit gates implemented using the SW and TW with the same duty cycle. We obtain errors of $1.44(3) \times 10^{-3}$ and $1.73(3) \times 10^{-3}$ per Clifford gate, respectively. Thus, use of the SW is not detrimental to single-qubit control.

Next, we experimentally investigate the saturation effect caused by the noncommuting carrier coupling [Eq. (3)] when generating an SDF with a bichromatic TW, and compare it to the SDF generated by a bichromatic SW. To create the TW bichromatic field, we apply two tones to the AOM in b_1, while for the SW we apply the same two tones in both beams, b_1 and b_2. These tones are symmetrically detuned by $\delta \approx \pm\omega_z$ from the qubit resonance. This results in an SDF on the axial mode ($\omega_z/2\pi \approx 1.2$ MHz) of a single ion. We extract its strength $\Omega_{\text{SDF}}(\Omega, \delta)$ by applying the SDF for variable durations [30]. We used an adiabatic ramp duration of 3.6 μs for these measurements [34].

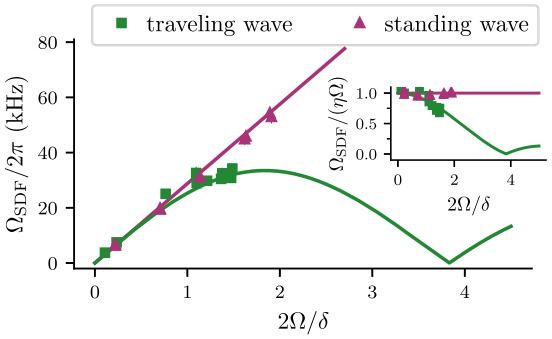

FIG. 3. Spin-dependent force magnitude Ω_{SDF} (normalized by $\eta\Omega$ in the inset) versus $2\Omega/\delta$, as measured for a single ion with $\eta = 0.051$. We extract Ω_{SDF} by applying a conventional bichromatic TW field (squares), or a bichromatic SW field (triangles), for variable durations. The solid lines show the analytical dependence; as predicted by the theory and shown explicitly in the inset, the TW coupling follows the Bessel functions ($|J_0 + J_2|$), while the SW coupling remains constant [35].

For the TW, we observe a coupling that scales with the expected Bessel function dependence $|J_0(2\Omega/\delta) + J_2(2\Omega/\delta)|$ [Eq. (4), Fig. 3]. Hence, when using the TW, there exists a maximum achievable interaction strength that imposes a speed limit on the interaction regardless of the available laser power. This limit is caused by the increasingly strong off-resonant noncommuting carrier excitation and not by technical aspects such as pulse shaping. For the SW, we demonstrate that no such speed limit exists. We place the ion at the maximum intensity of both the RD and BD SWs [27] and observe that the interaction magnitude [35] increases linearly with Ω (Fig. 3).

An important application of a bichromatic SW is to generate strong SDFs without any off-resonant carrier excitation. This can then be combined with pulse-segmentation techniques [16,36,37] to enable fast, nonadiabatic entangling operations. Additionally, undesired squeezing terms $\mathcal{O}(\eta^2)$, which were the dominant source of error in the fastest previous implementation [16], are suppressed [27].

We experimentally demonstrate two-qubit MS gates using a bichromatic TW for gate speeds in a regime where the carrier coupling induces a significant error which cannot be eliminated adiabatically. However, the bichromatic SW enables us to surpass this limit without degradation of the fidelity (Fig. 4). To implement the SW-MS gate, we simultaneously suppress the carrier coupling on both ions by adjusting the ion spacing such that they are both located at antinodes of the SW [Fig. 1(c)] [27]. We perform the TW and SW two-qubit entangling gates on the axial in-phase mode and optimize the experimental parameters to maximize the Bell-state fidelity for a fixed gate duration. In both cases, we use a ramp duration of 10 μs to minimize coupling to the other motional modes [34]. This pulse ramping could be replaced with more sophisticated amplitude shaping techniques [16,36,37].

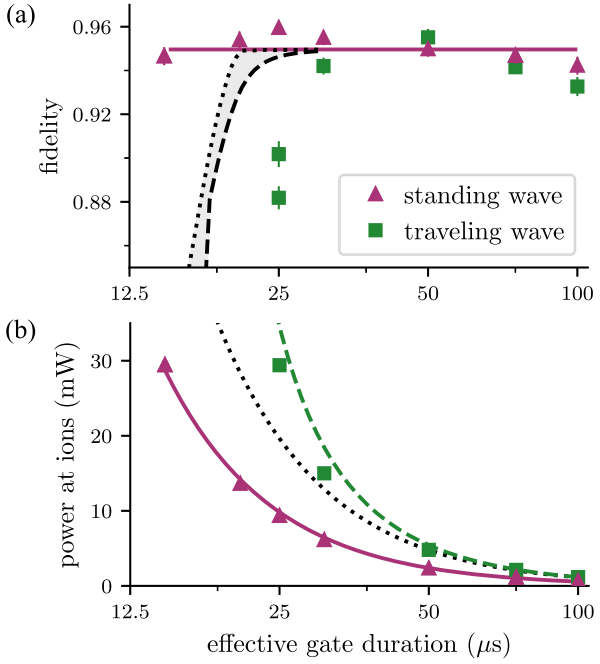

FIG. 4. Characterization of SW (triangles) and TW (squares) Mølmer-Sørensen gates as a function of the effective two-qubit gate duration ($2\pi/\delta_g$). (a) Using the SW, we achieve gate fidelities that are consistent with ≈0.95 (solid line) for all gate durations. Using the TW the fidelity decreases rapidly for durations ≤ 25 μs. As a guide to the eye, we show TW-MS simulations (dotted and dashed lines), with the maximum fidelity normalized to 0.95. (b) Total laser power required at the ions to generate the gate interaction. The constructive interference of the SW reduces the required power at the ions by a factor of 2. The solid curve shows an inverse-square fit to the SW data. We scale this curve by a factor of 2 (dotted line) for comparison with the TW data. At fast gate durations (≲40 μs), the required power for TW gates exceeds this prediction as a result of the saturation of the SDF (Fig. 3). We scale this prediction by the expected Bessel function dependence (dashed line) and find good agreement with the measurements.

In Fig. 4(a) we show the two-qubit fidelities achieved with the two schemes as a function of the effective gate duration ($2\pi/\delta_g$, where $\delta_g = \delta - \omega_z$) [38]. For slower gates, the fidelity of the SW-MS is comparable with that of the TW-MS. For faster gates, the fidelity of the TW-MS degrades rapidly. This is also predicted by direct numerical integration of Eq. (3); we set all the parameters to the experimental values except for the Rabi frequency Ω, which we optimize for maximum fidelity (dashed line). We also indicate the idealized case which neglects imperfect transfer into the interaction picture w.r.t. the carrier [Eq. (3)] (dotted line). We believe that the measured fidelities degrade sooner (by ≈5 μs) as a result of experimental imperfections (e.g. in ramp shape) not captured in the numerical model. In contrast, the fidelity for the SW-MS is consistent with ≈0.95 over the entire available power range, showing that we have eliminated the limit arising from the

carrier coupling. The shortest SW-MS gate was 15 μs, limited by the total available laser power of 29 mW.

In Fig. 4(b), we plot the total laser power delivered to the ions as a function of the effective gate duration. For the SW, the total required power (b_1 and b_2 summed) closely follows an inverse-square law. For a given duration, the TW-MS requires significantly more power than the SW-MS: the interference effect between the counterpropagating beams gives the SW-MS a factor of 2 increase in power efficiency; the saturation effect (Fig. 3) further increases the TW-MS power requirement.

We believe the main source of infidelity for entangling operations is phase noise from the 674-nm laser, which is common to both gate implementations. We estimate the sources of error that are introduced by the SW in the Supplemental Material [27]: the visibility error due to amplitude imbalance between beams b_1 and b_2; the quality of the SW phase stabilization, which introduces a position jitter of the SW relative to the ions; mismatched spacing of the ions relative to the SW periodicity; and phase misalignment of the BD and RD SWs ($\Delta\phi_{\mathrm{BD}} \neq 0$ or $\Delta\phi_{\mathrm{RD}} \neq 0$). The total error introduced is $< 9 \times 10^{-3}$ for a square pulse and $< 2 \times 10^{-5}$ when using a shaped pulse, which suppresses carrier related errors by 3 orders of magnitude and is employed for the results presented in Fig. 4.

In conclusion, we implemented single- and two-qubit operations for trapped-ion qubits using a phase-stabilized SW. Two counterpropagating beams create the SW, whose relative phase $\Delta\phi$ at the ion position is stable to $\approx\lambda/100$. This enabled us to tune the ratio of the field intensity and gradient that the ions experience, which sets the relative strengths of the sideband and carrier interactions. We use this new degree of control to suppress the unwanted off-resonant carrier coupling (by a factor of 18), while coherently enhancing the motional coupling during two-qubit gates. We show theoretically and experimentally that the noncommuting carrier term imposes a limit on the speed of conventional TW-MS gates, which we circumvented by using the SW-MS interaction. These optical phase control techniques could also be applied in the previous Raman-based scheme [16], where they could mitigate squeezing terms, which were the leading error source; we note that for the SW-MS those terms are inherently suppressed. Our Letter shows a clear path toward entangling gates with durations shorter than the motional period of the ions ($\lesssim 1$ μs) at wavelengths that are amenable to large-scale chip integration using standard integrated optics [39–41] and without the technical challenges of using high-power blue Raman beams [16], pulsed lasers [42,43], or Rydberg schemes [44].

We would like to thank V. M. Schäfer, A. C. Hughes, and D. P. Nadlinger for thoughtful discussions. This work was supported by the U.S. Army Research Office (W911NF-20-1-0038) and the UK EPSRC Hub in Quantum Computing and Simulation (EP/T001062/1). C. J. B. acknowledges support from a UKRI FL Fellowship. R. S. acknowledges funding from the EPSRC Fellowship EP/W028026/1 and Balliol College, Oxford. G. A. acknowledges support from Wolfson College, Oxford.

G. A. consults for Nu Quantum Ltd. R. S. is partially employed by Oxford Ionics Ltd. C. J. B. is a director of Oxford Ionics Ltd. All other authors declare no competing financial interests.

*sebastian.saner@physics.ox.ac.uk
†oana.bazavan@physics.ox.ac.uk
‡These authors contributed equally to this work.

[1] J. I. Cirac and P. Zoller, Phys. Rev. Lett. **74**, 4091 (1995).
[2] C. Monroe, D. M. Meekhof, B. E. King, W. M. Itano, and D. J. Wineland, Phys. Rev. Lett. **75**, 4714 (1995).
[3] D. J. Wineland, C. Monroe, W. M. Itano, D. Leibfried, B. E. King, and D. M. Meekhof, J. Res. Natl. Inst. Stand. Technol. **103**, 259 (1998).
[4] R. Blatt and C. F. Roos, Nat. Phys. **8**, 277 (2012).
[5] D. Jaksch and P. Zoller, Ann. Phys. (Amsterdam) **315**, 52 (2005), special Issue.
[6] P. O. Schmidt, T. Rosenband, C. Langer, W. M. Itano, J. C. Bergquist, and D. J. Wineland, Science **309**, 749 (2005).
[7] F. Wolf, Y. Wan, J. C. Heip, F. Gebert, C. Shi, and P. O. Schmidt, Nature (London) **530**, 457 (2016).
[8] R. Blatt and D. Wineland, Nature (London) **453**, 1008 (2008).
[9] A. B. Mundt, A. Kreuter, C. Becher, D. Leibfried, J. Eschner, F. Schmidt-Kaler, and R. Blatt, Phys. Rev. Lett. **89**, 103001 (2002).
[10] T. E. DeLaubenfels, K. A. Burkhardt, G. Vittorini, J. T. Merrill, K. R. Brown, and J. M. Amini, Phys. Rev. A **92**, 061402 (2015).
[11] A. R. Vasquez, C. Mordini, C. Vernière, M. Stadler, M. Malinowski, C. Zhang, D. Kienzler, K. K. Mehta, and J. P. Home, Phys. Rev. Lett. **130**, 133201 (2023).
[12] C. T. Schmiegelow, H. Kaufmann, T. Ruster, J. Schulz, V. Kaushal, M. Hettrich, F. Schmidt-Kaler, and U. G. Poschinger, Phys. Rev. Lett. **116**, 033002 (2016).
[13] A. Sørensen and K. Mølmer, Phys. Rev. A **62**, 022311 (2000).
[14] K. K. Mehta, C. Zhang, S. Miller, and J. P. Home, Proc. SPIE Int. Soc. Opt. Eng. **10933**, 109330B (2019).
[15] D. Kielpinski, C. Monroe, and D. J. Wineland, Nature (London) **417**, 709 (2002).
[16] V. M. Schäfer, C. J. Ballance, K. Thirumalai, L. J. Stephenson, T. G. Ballance, A. M. Steane, and D. M. Lucas, Nature (London) **555**, 75 (2018).
[17] B. Reznik, A. Retzker, and J. Silman, Phys. Rev. A **71**, 042104 (2005).
[18] A. Retzker, J. I. Cirac, and B. Reznik, Phys. Rev. Lett. **94**, 050504 (2005).
[19] M. Drechsler, S. Wolf, C. T. Schmiegelow, and F. Schmidt-Kaler, Phys. Rev. Lett. **127**, 143602 (2021).

[20] Z.-H. Qian, J.-M. Cui, X.-W. Luo, Y.-X. Zheng, Y.-F. Huang, M.-Z. Ai, R. He, C.-F. Li, and G.-C. Guo, Phys. Rev. Lett. **127**, 263603 (2021).

[21] V. I. Yudin, A. V. Taichenachev, C. W. Oates, Z. W. Barber, N. D. Lemke, A. D. Ludlow, U. Sterr, C. Lisdat, and F. Riehle, Phys. Rev. A **82**, 011804(R) (2010).

[22] A. N. Vetlugin, R. Guo, C. Soci, and N. I. Zheludev, Phys. Rev. A **106**, 012402 (2022).

[23] J. I. Cirac, R. Blatt, A. S. Parkins, and P. Zoller, Phys. Rev. Lett. **70**, 762 (1993).

[24] J. I. Cirac, R. Blatt, A. S. Parkins, and P. Zoller, Phys. Rev. A **49**, 1202 (1994).

[25] Y. Wu and X. Yang, Phys. Rev. Lett. **78**, 3086 (1997).

[26] $\hat{\sigma}_\alpha^{(i)} = \underbrace{\hat{\mathbb{I}}_2 \otimes \ldots \otimes \hat{\mathbb{I}}_2}_{i-1} \otimes \hat{\sigma}_\alpha \otimes \underbrace{\hat{\mathbb{I}}_2 \otimes \ldots \otimes \hat{\mathbb{I}}_2}_{n-i}$, where $\alpha \in \{+, -, x, y\}$ in this Letter.

[27] See Supplemental Material at http://link.aps.org/supplemental/10.1103/PhysRevLett.131.220601 for additional steps in the derivation of the equations presented in the text and for experimental details.

[28] C. F. Roos, New J. Phys. **10**, 013002 (2008).

[29] R. Sutherland, R. Srinivas, S. C. Burd, D. Leibfried, A. C. Wilson, D. J. Wineland, D. Allcock, D. Slichter, and S. Libby, New J. Phys. **21**, 033033 (2019).

[30] O. Băzăvan, S. Saner, M. Minder, A. C. Hughes, R. T. Sutherland, D. M. Lucas, R. Srinivas, and C. J. Ballance, Phys. Rev. A **107**, 022617 (2023).

[31] K. Thirumalai, Ph.D. thesis, University of Oxford, 2019.

[32] V. Schäfer, Ph.D. thesis, University of Oxford, 2018.

[33] E. Knill, D. Leibfried, R. Reichle, J. Britton, R. B. Blakestad, J. D. Jost, C. Langer, R. Ozeri, S. Seidelin, and D. J. Wineland, Phys. Rev. A **77**, 012307 (2008).

[34] The ramp shape is a $\sin(\pi t/2t_R)^2$ with a total rise time given by the ramp duration t_R.

[35] Note that Ω in $\Omega_{\mathrm{SDF}}(\Omega, \delta)$ for the SW has been rescaled by a factor of 2 to account for the power enhancement due to interference, and in order to compare fairly the TW to the SW.

[36] A. M. Steane, G. Imreh, J. P. Home, and D. Leibfried, New J. Phys. **16**, 053049 (2014).

[37] M. Palmero, S. Martínez-Garaot, D. Leibfried, D. J. Wineland, and J. G. Muga, Phys. Rev. A **95**, 022328 (2017).

[38] The effective gate duration is approximately equal to the full-width at half maximum of the pulse shape. The pulse duration from start to end is $2\pi/\delta_g + t_R$, where t_R is the ramp duration. The ramp shape is as defined in [34].

[39] S. X. Wang, G. Hao Low, N. S. Lachenmyer, Y. Ge, P. F. Herskind, and I. L. Chuang, J. Appl. Phys. **110**, 104901 (2011).

[40] R. J. Niffenegger, J. Stuart, C. Sorace-Agaskar, D. Kharas, S. Bramhavar, C. D. Bruzewicz, W. Loh, R. T. Maxson, R. McConnell, D. Reens, G. N. West, J. M. Sage, and J. Chiaverini, Nature (London) **586**, 538 (2020).

[41] K. K. Mehta, C. Zhang, M. Malinowski, T.-L. Nguyen, M. Stadler, and J. P. Home, Nature (London) **586**, 533 (2020).

[42] J. J. García-Ripoll, P. Zoller, and J. I. Cirac, Phys. Rev. Lett. **91**, 157901 (2003).

[43] J. D. Wong-Campos, S. A. Moses, K. G. Johnson, and C. Monroe, Phys. Rev. Lett. **119**, 230501 (2017).

[44] C. Zhang, F. Pokorny, W. Li, G. Higgins, A. Pöschl, I. Lesanovsky, and M. Hennrich, Nature (London) **580**, 345 (2020).